Effect of supercritical CO2 plasticization on the degradation and residual crystallinity of melt-extruded spironolactone

Tamas Vigh, Martial Sauceau, Jacques Fages, Élisabeth Rodier, Istvan Wagner, Peter L. Soti, Gyoergy Marosi, Zsombor K. Nagy

Effect of supercritical CO_2 plasticization on the degradation and residual crystallinity of melt-extruded spironolactone

Tamás Vigh[a], Martial Sauceau[b], Jacques Fages[b], Elisabeth Rodier[b], István Wagner[a], Péter L. Sóti[a], György Marosi[a]* and Zsombor K. Nagy[a]

Immediate-release solid dispersions of a slowly dissolving active pharmaceutical ingredient, spironolactone, were prepared by supercritical-CO_2-assisted melt extrusion (a solvent-free and continuous manufacturing technology) using Eudragit E as matrix. Through optimizing process parameters (i.e. temperature, melt throughput, pressure and CO_2 flow), stable foams with high porosity, homogeneous structure and thin (even submicronic) walls could be prepared, as revealed by scanning electron microscopy. The samples were found to be rigid enough to mill, enabling further processing, as is necessary to formulate tablets. The influence of extrusion temperature and melt throughput on residual drug crystallinity was measured using non-invasive confocal Raman mapping coupled with chemometric analysis, while the influence on the degree of drug degradation was determined using high performance liquid chromatography. The plasticizing effect of supercritical CO_2 was shown to reasonably improve the purity of the prepared solid dispersions by enabling high-yield production at lower temperature ranges. At the same time, shorter residence time and lower temperature slightly increased residual drug crystallinity. The obtained foamy structures ensured immediate drug dissolution in an acidic medium.

Keywords: supercritical-fluid extrusion; foaming; immediate release; degradation; amorphization

INTRODUCTION

Melt extrusion is a well-known technique used to disperse poorly water-soluble crystalline active pharmaceutical ingredients (APIs) in polymers in order to accelerate their dissolution.[1] At the same time, it can also enhance bioavailability.[2–5] The API can be dissolved in the polymer melt in the course of extrusion; therefore, there is no crystal lattice to be destructed during the dissolution of the formulation in the stomach. Dissolution of the API from the resulting solid suspensions or solid solutions can be faster for several reasons. First, the solubility of the amorphous form is higher than that of the crystalline forms.[6] Second, matrix polymers can ensure better wettability and also solubilize drug molecules, thus improving their apparent solubility.

Regarding the production of solid dispersions, solvent-free, high-throughput continuous manufacturing technologies (such as melt extrusion) are recommended by process analytical technology (PAT) guidelines[7] and have a wide range of dosage forms (mini matrices, granules, pellets, foams, films and implants).[3] On the other hand, a clear disadvantage of melt extrusion is that most pharmaceutical-grade polymers can only be processed at a high temperature due to their high glass-transition temperature (T_g) or melting point (T_m). Despite the growing number of the marketed pharmaceutical products that are produced by melt extrusion (for example Kaletra® and Isoptin SR-E®[8–10]), the heat sensitivity of some active compounds can be an obstacle to the application of melt granulation methods. Purity improvement of melt extruded dosage forms is a rarely chosen objective of relevant research papers, and even literature evaluation of API degradation in the course of melt extrusion is limited to a few chemical compounds, such as hydrocortisone,[11] carbamazepine, dipyridamole and indomethacin,[12] meloxicam[13] and vitamin D.[14] API decomposition does not necessarily mean thermal degradation; it can also be initiated by free radicals.[11] *Krupa et al*. have proved that salt formation can be a way to enhance API stability,[15] while other compounds can be stabilized against thermal stress by complexation with cyclodextrins.[16] Additionally, moderation of the thermal stress can solve purity issues at their roots. Plasticization is mostly needed in order to decrease temperature and shorten residence time, both of which can have influence on the degree of degradation.[11,13] However, plasticizers remaining in the extrudate permanently lower its glass-transition temperature (T_g), making further processing impossible or circumstantial, and often reducing physical stability.

An interesting alternative of plasticization achieved through the addition of organic substances (irreversible plasticizers) is the injection and dissolution of supercritical carbon dioxide ($scCO_2$) into the molten polymer conveyed in the extruder.[17]

* *Correspondence to: György Marosi, Budapest University of Technology and Economics, Department of Organic Chemistry and Technology, 1111 Budapest, Műegyetem rkp. 3 9, FII. mfsz. 17, Hungary.*
E mail: gmarosi@mail.bme.hu

a *T. Vigh, I. Wagner, P. L. Sóti, G. Marosi, Z. K. Nagy*
Budapest University of Technology and Economics, Department of Organic Chemistry and Technology, 1111 Budapest, Budafoki út 8, Hungary

b *M. Sauceau, J. Fages, E. Rodier*
Université de Toulouse, École des Mines d'Albi, CNRS, Centre RAPSODEE, F 81013, Albi, France

By enabling production at a lower temperature and high melt throughput,[18] it can reduce decomposition of thermally instable compounds, as shown by *Verreck et al*.[19] Special attention is given to this substance because it does not remain in the extrudate after processing. Therefore, it only modifies the rheological properties of the polymer during extrusion—the plasticizing effect ceases afterwards, leaving behind a well-grindable, rigid product with high T_g. $ScCO_2$ can also be used as a physical blowing agent owing to the gaseous CO_2 bubbles nucleating and growing in the melt after pressure has dropped through the extruder die. Growth of these pores continues until the extrudate rigidifies or until the whole amount of CO_2 diffuses into the atmosphere. There are no notable environmental concerns regarding the application of $scCO_2$,[20] and this blowing agent leaves no residue in the foams; therefore, it can be used in pharmaceutical and food products.[21,22] $ScCO_2$- and pressurized-CO_2-assisted extrusion in particular has already been used to manufacture a wide range of products in these two industrial areas as *Rizvi et al*.[23] and *Sauceau et al*.[24] pointed out, but the technology has not yet been employed for dissolution enhancement, save for a couple of studies.[17,25,26] The relationship between amorphization and drug degradation remains unclear. The high specific surface area generated by the foaming process can be extremely beneficial in the case of immediate release formulations because it greatly influences dissolution rate.[27,28]

This study was aimed to examine whether the plasticizing effect of $scCO_2$ can reduce degradation of a thermally instable model API, spironolactone, in the course of melt extrusion with Eudragit E. The rationale for this examination was that the statistical cationic copolymer Eudragit E (which is commonly used as an immediate-release extrusion matrix) can only be processed at high temperature (typically at and above 130°C) without plasticization,[29] but spironolactone (Fig. 1A) partially decomposes to canrenone (Fig. 1B) in this temperature range, as shown previously (data not given). This purity issue can be an obstacle to conventional extrusion processing of this system, which could otherwise enhance the slow dissolution of the drug compound.

It was also investigated how much the milder conditions established by $scCO_2$ hindered API dissolution in the melt and hence increased residual drug crystallinity, which can affect product quality. In order to obtain exact information on purity and crystallinity, extrudates were analyzed using high performance liquid chromatography (HPLC) and non-invasive confocal Raman mapping coupled with chemometrics, respectively. It has already been proven that Raman spectrometry can be used to determine chemical composition,[30] quantify polymorphs (including the amorphous form) in a mixture,[31–34] measure the degree of crystallinity[35] and investigate the distribution of amorphous and crystalline material[36,37] in solid samples. Raman spectrometry is a potential PAT tool enabling in-line monitoring and feedback control, as recently shown by *Pataki et al*.[38,39] Another goal of this study was to investigate the influence of extrusion parameters on foam structure and find the conditions delivering homogeneous extrudates with the thinnest possible cell walls.

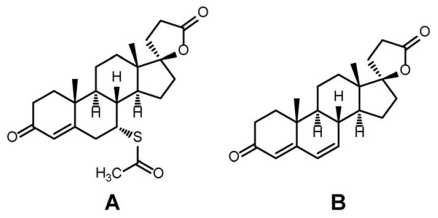

Figure 1. Chemical structure of (A) spironolactone and (B) canrenone.

EXPERIMENTAL

Materials

Microcrystalline spironolactone, which has a molar mass of 417 g/mol, a melting range of 207–216°C, an average particle size of approx. 30 μm, an octanol logP of 2.6[40] and a water solubility of 28 mg/l at 25°C[41] was kindly supplied alongside canrenone (m.w. 340 g/mol) and Δ20-spironolactone (m.w. 415 g/mol) by Gedeon Richter Plc. (Budapest, Hungary). Eudragit® E 100, a cationic copolymer based on dimethylaminoethyl methacrylate, butyl methacrylate and methyl methacrylate, with an average molecular weight of 47,000 Da and a glass transition temperature of 62°C was obtained from Evonik Industries AG (Essen, Germany).

Melt extrusion

Supercritical-CO_2-aided melt extrusion of a mixture of 10% spironolactone and 90% Eudragit E was performed on a single-screw extruder (SCAMEX, Crosne, France), details of which can be found in literature.[42] Hopper temperature was fixed at 50°C. Barrel temperature was controlled separately in five zones: T_1 and T_2 before the CO_2 injection point, T_3 and T_4 after it, while T_5 was the temperature of the die. T_1 was fixed at 100°C for all experiments, while T_2–T_5 had always the same value, which is hereafter simply referred to as temperature, T. Temperature of the melt was measured at two points: T_{m1} between the zones T_3 and T_4, and T_{m2} in the die. Extrudates were cooled with compressed air at ambient temperature after leaving the die. Screw speed was adjusted to a value that ensured the desired melt throughput (mass flow rate). Pressure was measured in four different points: P_1 in the CO_2 injection point, P_4 in the die, P_2 and P_3 between the two previous points. Pressure profile was controlled by constricting the cross-sectional area of the channel in a home-made die by means of a central pin. The pressure profile is characterized by the value of P_4 in this article. CO_2, which had been cooled to 5°C, was pumped into the barrel with a constant volumetric flow rate using a pressure bearing syringe pump (260D, ISCO, Lincoln, NE, USA). CO_2 density obtained from the website of NIST[43] and calculated with the Span and Wagner equation of state[44] was used to determine the CO_2 mass flow rate and the CO_2 mass percentage in the melt.

Table 1 displays the extrusion conditions for all prepared spironolactone formulations. Concerning melt throughput and the mass percent of CO_2 in the melt, comparison-aiding groups were defined; each group contained extrudates with similar values. The measured values of these variables are also given in brackets. Sample names were composed from extrusion parameters (rounded, without units) in the order of prefix, temperature, melt throughput, P_4, and CO_2 percentage, separated by slashes: e.g. S 110/1/250/6.

Measurement of drug degradation

The degree of spironolactone to canrenone degradation in the extrudates was determined using HPLC. Ground extrudates were dissolved (nominally 1 mg of spironolactone/ml) in a 1:1 mixture of methanol and 0.1 M acetic acid. Twenty microliters of the solution were isocratically chromatographed on an Agilent Eclipse

Table 1. Extrusion parameters of spironolactone solid dispersions prepared using $scCO_2$-aided and conventional melt extrusion. Composition: 10% spironolactone, 90% Eudragit E

Sample	T (°C)	T_{m1}–T_{m2} (°C)	Throughput (g/min)	P_4 (bar)	CO_2 mass percent (%)	Torque (N m)
S 130/1/250/0	130	134–121	1.3 ± 0.5 (1.67)	250	0.00	123
S 120/1/250/0	120	124–114	1.3 ± 0.5 (0.85)	250	0.00	158
S 130/10/150/3	130	135–124	9.7 ± 0.9 (9.41)	150	2.7 ± 0.8 (2.10)	100
S 110/10/150/3	110	113–106	9.7 ± 0.9 (8.80)	150	2.7 ± 0.8 (2.24)	173
S 130/10/200/3	130	135–124	9.7 ± 0.9 (9.45)	200	2.7 ± 0.8 (2.10)	132
S 130/10/250/3	130	135–124	9.7 ± 0.9 (10.45)	250	2.7 ± 0.8 (1.90)	145
S 130/10/250/6	130	135–124	9.7 ± 0.9 (10.03)	250	6.3 ± 0.8 (5.70)	143
S 130/1/250/6	130	134–122	1.3 ± 0.5 (1.75)	250	6.3 ± 0.8 (5.46)	145
S 110/6/200/3	110	113–106	6.4 ± 0.7 (7.07)	200	2.7 ± 0.8 (2.78)	174
S 110/6/250/3	110	114–107	6.4 ± 0.7 (5.67)	250	2.7 ± 0.8 (3.44)	205
S 110/6/250/6	110	114–106	6.4 ± 0.7 (5.80)	250	6.3 ± 0.8 (6.51)	193
S 110/1/250/6	110	114–106	1.3 ± 0.5 (1.34)	250	6.3 ± 0.8 (7.01)	151

XDB-C18 5 μm (4.6 mm × 150 mm) column thermostated to 40°C, using an Agilent 1200 HPLC coupled with an Agilent 6130 Quadrupole MS system (Santa Clara, California, USA). The eluent had the following composition: 1.5% acetonitrile, 2.0% tetrahydrofurane, 42.5% methanol and 54.0% 0.1 M acetic acid, while it had a flow rate of 0.4 ml/min.

Detected compounds were identified by their characteristic MS peaks as well as their UV absorption peaks. It was found that the prevalent and, in most cases, the only decomposition product of spironolactone was canrenone. Therefore, the degree of drug degradation (x_d) could be calculated as the molar concentration of canrenone divided by the sum of canrenone and spironolactone molar concentrations. Molar ratios of spironolactone and canrenone were calculated from the peak areas in 254-nm UV chromatograms. The difference in the molar extinctions of spironolactone and canrenone was taken into account by means of calibration.

Measurement of foam porosity

Porosity (ε) of foams was calculated from their apparent density (ρ_{app}) and the density of a non-foamed extrudate (ρ) as $\varepsilon = 1 \quad (\rho_{app} \ / \ \rho)$. ρ_{app} was determined from weight and dimensional measurements (repeated 3 times using different parts of the samples), while ρ was measured using helium pycnometry (AccuPYC 1330, Micromeritics, Norcross, GA, USA). Owing to the die geometry, a wide empty channel was present in the middle of solidified extrudates, which was excluded from calculations and was not considered to be part of the foams.

Scanning electron microscopy

Morphology of samples was investigated by a JEOL 6380LVa (JEOL, Tokyo, Japan) type scanning electron microscope (SEM). Each specimen was fixed by conductive double-sided carbon adhesive tape and sputtered with gold (using a JEOL 1200 instrument) in order to avoid electrostatic charging. Cell density (n) of foams was calculated from the cell number on SEM images (N), the scanned area (A) and the densities defined in the experimental section, using the formula below. Value n expresses the number of cells that have evolved in a volumetric unit of the non-foamed melt.

$$n = \left(\frac{N}{A}\right)^{3/2} \cdot \frac{\rho}{\rho_{app}}$$

Three-point bending

Three-point bending was carried out with a Q800 (TA Instruments, New Castle, DE, USA) dynamic mechanical analyzer at room temperature with cylindrical sample geometry, using a preload force of 0.001 N. The load was increased continuously with a rate of 3 N/min until the fracture of the sample or up to 18 N.

X-ray powder diffraction

Ground extrudates and starting materials were investigated with a PANalytical X'pert Pro MPD X-ray diffractometer (Almelo, the Netherlands) equipped with an X'Celerator detector with 0.04 sollers, using Cu Kα radiation (1.542 Å) and a Ni filter. The applied voltage and current were 40 kV and 30 mA, respectively. The samples were analyzed between 4° and 42° 2θ. Automatic divergence and anti-scatter slits were used to provide an irradiated length of 20 mm.

Confocal Raman mapping

Backscattering Raman spectra were collected using a Horiba Jobin-Yvon LabRAM system coupled with an external 785-nm diode laser source (spot size: 200 μm) and an Olympus BX-40 optical microscope. A confocal objective of 10× magnification was used. Non-ground extrudates were compressed into flat discs (Camilla OL95, Manfredi, Torino, Italy), and their surface was mapped in 10 × 10 equidistant points, 150 μm away from each other, in order to avoid subsampling. Acquisition, spectrum processing and visualization of maps were performed using LabSpec 5.41 (Horiba Jobin-Yvon) software.

The mean spectrum was baseline-corrected and subjected to modeling steps, which were performed with the method of classical least squares (CLS). The spectroscopic concentrations (scores) of canrenone and spironolactone were computed based on the spectral range between 1550 and 1800 cm^{-1}, using the spectra of pure Eudragit E, canrenone, crystalline and amorphous spironolactone, which had been collected on the same device under the same conditions. Amorphous spironolactone was prepared by electrospraying, and the spectrum of crystalline canrenone was used as an approximation (based on HPLC measurements, canrenone could be considered to be the only decomposition product that was present in a significant amount in the extrudates).

As the spectra of the amorphous and crystalline API were quite similar regarding overall intensity and Raman shifts, the accurate determination of their ratio was performed based on the range between 1685 and 1695 cm^{-1} of the first derivative spectrum, in which there was a characteristic and well-measurable difference between the two forms. As the spectral intensities of the two forms were very similar, component spectra were not normalized.

In vitro drug dissolution

The dissolution measurements were performed on a PTWS 600 dissolution tester (USP II apparatus, Pharma Test Apparatebau AG, Hainburg, Germany). Ground extrudates ($0.4\,mm < d_p < 0.8\,mm$) equivalent to 8 mg of spironolactone were placed in the dissolution vessel, which had been filled with 900 ml of 0.1 M hydrochloric acid maintained at (37.0 ± 0.5) °C and stirred at 100 rpm. Samples were taken after 0, 1, 2, 3, 4, 5, 6, 7, 8, 9, 10, 15, 20, 25, 30, 45, 60, 75, 90, 105 and 120 min (washing period prior to sampling was 30 s) and were analyzed on-line using a Hewlett-Packard HP 8453G UV–VIS spectrophotometer (Palo Alto, USA) at 242 nm, using a diode array detector, then added back to the dissolution vessel.

RESULTS AND DISCUSSION

Purity enhancement

In this study, it was investigated how supercritical-fluid-assisted melt extrusion can help to reduce the degradation of a heat-sensitive API in the course of melt processing while maintaining good grindability by avoiding the application of conventional plasticizers, which remain in the extrudate and keep glass-transition temperature low. Spironolactone, which belongs to Class II of the Biopharmaceutics Classification System (BCS) and is thermally sensitive when not maintained in a crystal lattice, was chosen as model drug. The statistical cationic copolymer Eudragit E was selected as a matrix because of its fast dissolution in acidic medium, good extrudability[45] and high miscibility with spironolactone. The interaction between the API and the monomers was calculated using the functional group contribution method of Hoftyzer and van Krevelen.[46] The solubility parameters were found to be close for the two materials ($\Delta\delta = 4.03\,MPa^{1/2}$). An API can be expected to be well-soluble in the matrix when $\Delta\delta$ is smaller than $5.0\,MPa^{1/2}$; thus, it was anticipated that Eudragit E would enable the formation of spironolactone molecular dispersions even in the case of high drug loadings.

Chromatographic examinations of preliminary extrudates showed that by far the main decomposition product of spironolactone was canrenone. Therefore, the spironolactone to canrenone conversion was investigated. Three samples from different points of each extruded formulation were tested by HPLC. The molecularly dispersed drug fraction is more likely subject to degradation in the course of high-temperature manufacturing than the crystals, which have a stabilizing lattice, and thus the amount of API which is degraded can depend on temperature and residence time. Consequently, extrusion was carried out at various conditions, which are described in details in experimental Section. A 10%-API mixture was first extruded without supercritical carbon dioxide ($scCO_2$). The optimal temperature of extrusion was 130°C (S 130/1/250/0, Table 1), while melt temperature was difficult to decrease to 120°C (S 120/1/250/0), and without $scCO_2$, extrusion was impossible at 110°C. Processing at 130°C and approx. 1 g/min throughput resulted in a 25.9% degradation (x_d) as shown in Table 2 (x_d denotes the mole percentage of spironolactone that degraded to canrenone).

x_d decreased reasonably to 7.3% for the plasticized system S 130/10/150/3, which was extruded at an increased melt throughput (and hence shorter residence time). Injection of the supercritical fluid also made it possible to have foam extrusion at 110°C with constant quality and without difficulty, and x_d decreased further to 5.5% (S 110/10/150/3). At this temperature, purity did not decrease notably even with increased residence time: 6.0% of spironolactone decomposed to canrenone in the case of S 110/6/250/6 (at 200 and 250-bar pressures, the maximum throughput was 6 g/min at 110°C because of the increased torque). The plasticized melt was also extrudable at 100°C, but the highest possible throughput of the viscous melt was only 0.7 g/min, which is not desirable from an industrial point of view. Therefore, the lowest extrusion temperature was 110°C in this study.

The slight standard deviations displayed in Table 2 suggest that the degraded API distribution in the products was homogeneous. Decreasing temperature and increasing throughput, made possible by using $scCO_2$, resulted in the dramatic purity enhancement of melt extruded products. The resulting foams, which had high specific surface area and contained the API finely dispersed were supposed to enhance the dissolution of the BCS II drug. The results of these measurements are discussed hereafter.

Foam structure

Foam morphology on fractured cross sectional surfaces was examined visually by scanning electron microscopy (SEM). In order to characterize the foams with regard to cell diameters and wall thickness values, these two attributes were measured in 40–60 random points for each sample, using representative SEM images. Analysis of S 130/1/250/6 and S 110/1/250/6 was not carried out because their structure was too irregular). The histograms displaying the distribution of measured cell diameters and cell wall thicknesses can be seen in Fig. S1 and Fig. S2 of the online available supplementary material, respectively. In Table 3, distributions are described using the quartiles of the ranked sets (these are the three values that divide the ranked dataset into four equal groups, each group comprising a quarter of the data). The second quartile (the median) is given first, while the first and third quartiles are given in brackets. In addition to these, cell density and porosity were calculated as described in the experimental section.

Big differences could be observed in the structures of the initial two samples, prepared at 130 and 110°C (S 130/10/150/3, S 110/10/150/3, Table 3, Fig. 2A and 2B). Extrusion at higher temperature resulted in notably lower cell density and thicker cell walls, which can be explained by the higher diffusivity of CO_2 in the less viscous polymer melt, and hence a higher degree

Table 2. Mean degrees of drug degradation in different extruded foams, based on three repeated analyses

Temperature (°C)	Throughput (g/min)	Sample name	Drug degradation to canrenone, x_d (mol%)
130	1.67	S 130/1/250/0	25.9 ± 0.6
130	9.41	S 130/10/150/3	7.3 ± 0.3
110	8.80	S 110/10/150/3	5.5 ± 0.7
110	5.80	S 110/6/250/6	6.0 ± 0.8

Table 3. Structural features of extruded spironolactone–Eudragit E foams

Sample	Cell density[a] (cm^{-3})	Porosity (%)[b]	Characteristic cell diameters (μm)[c]	Characteristic wall thicknesses (μm)[c]
S 130/10/150/3	$3.8 \cdot 10^4$	75 ± 1	350 (249; 460)	17 (9; 42)
S 110/10/150/3	$1.6 \cdot 10^5$	92 ± 1	212 (146; 313)	2 (1; 5)
S 130/10/200/3	$1.8 \cdot 10^4$	80 ± 2	442 (227; 628)	6 (4; 16)
S 130/10/250/3	$3.7 \cdot 10^4$	80 ± 5	218 (115; 279)	10 (7; 19)
S 130/10/250/6	$2.4 \cdot 10^4$	83 ± 1	297 (164; 474)	7 (3; 9)
S 130/1/250/6	$2.6 \cdot 10^4$	64 ± 2	n/a	n/a
S 110/6/200/3	$1.7 \cdot 10^5$	92 ± 1	275 (186; 349)	2 (1; 4)
S 110/6/250/3	$6.6 \cdot 10^4$	85 ± 2	502 (377; 597)	11 (8; 20)
S 110/6/250/6	$8.6 \cdot 10^4$	87 ± 3	295 (220; 377)	5 (3; 9)
S 110/1/250/6	$2.0 \cdot 10^4$	85 ± 5	n/a	n/a

[a]Number of cells that formed in a volumetric unit of the non-porous melt.
[b]± standard deviation ranges are given based on three repetitions.
[c]Data are given as follows: median (first quartile; second quartile).

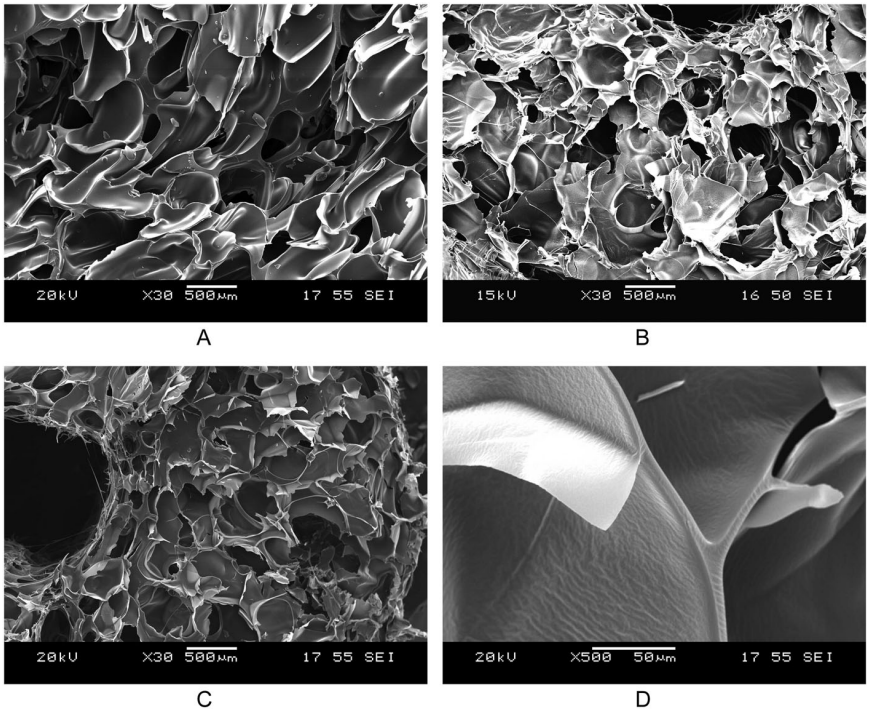

Figure 2. SEM images of (A) S 130/10/150/3, (B) S 110/10/150/3 and (C, D) S 110/6/200/3.

of coalescence in the course of pore formation. The cells were larger in the case of S 130/10/150/3, which is in correspondence with the earlier reported behavior of pure Eudragit E.[29]

At the same time, the decrease observed in porosity (from 92 to 75%) shows that at 130°C CO_2 diffused more easily to the atmosphere because of the low viscosity, resulting in contracted pores. Usually, the highest expansion can be reached when melt strength counterbalances blowing agent diffusion, which prevents the rupture of cells.[47] The diffusivity of the blowing agent and thereby the extension rate and strain associated with cell growth increase with temperature, while melt viscosity and elasticity show a reverse trend.[47] At 110°C pore contraction was also likely, because cell walls were thinner (the thinner the walls, the more CO_2 could escape). The reason why contraction was not so intense at 110°C as at 130°C can be that foams could keep their highly expanded structure because the surface of the extrudate was frozen faster at the lower die temperature. In fact, gas diffusion was hindered at the surface and so more gas remained in the foam to contribute to volume expansion, similarly as discussed in the literature.[48]

In the second and third series of experiments, the values of different extrusion parameters (pressure profile, CO_2 mass percentage and melt throughput) were varied in order to observe how these factors influenced foam structure at 130 and 110°C. For reliable analysis, samples differing only in one parameter were compared (Table 3).

Pressure profile, above all the value of P_4, was expected to affect the pore nucleation step. In the investigated range (150, 200 and 250 bar), a P_4 value of 200 bar was found to be optimal at both temperatures (S 130/10/200/3 and S 110/6/200/3), because this

setting resulted in high porosity and the thinnest cell walls (Table 3). Moreover, S 110/6/200/3 had the most beneficial attributes for an immediate-release formulation among all the prepared foams: an outstandingly homogeneous structure with 92% porosity, narrow cell diameter distribution and extremely thin (typically 1–4-μm-thick) cell walls (Fig. 2C and 2D). Many submicronic (500–700 nm) walls were also observed. The fact that the optimum pressure was 200 bar indicates a complex relationship between pressure drop and the phenomena involved in foaming, and that more than one step of the foaming process was modified by changing P_4.

An increase in the percentage of CO_2 was also found to be beneficial. In comparison with S 130/10/250/3 and S 110/6/250/3, porosity became slightly higher, and wall thicknesses more uniform and slightly narrower in the case of S 130/10/250/6 and S 110/6/250/6, respectively (Table 3, Fig. 3A and 3B). This is a clear indication that a major part of the injected CO_2 had sufficient time to diffuse and dissolve into the polymer melt. As no significant and unambiguous increase could be observed in cell density, this change can be attributed to an increased cell growth, with more gas being available in the nucleating phase to diffuse into the pores.

Finally, the effect of melt throughput was studied. At 130°C, throughputs of 1 and 10 g/min were set (S 130/1/250/6 and S 130/10/250/6), but at 110°C it could only be controlled between 1 and 6 g/min at a P_4 of 200 and 250 bar (S 110/1/250/6 and S 110/6/250/6). A decrease in melt throughput caused a reasonable decrease in pressure drop rate (the local derivative of pressure, $\partial P/\partial t$) and likely increased the possibility of gas diffusion through cells, which made the foams less uniform and the structure less predictable. At 110°C porosity did not depend on melt throughput, only the structure became inhomogeneous (S 110/1/250/6, Table 3), while at 130°C porosity decreased dramatically from 83 to 64% (S 130/1/250/6, Table 3) with the throughput decreasing from 10 to 1 g/min. Thick cell walls and irregular foam structure could be observed in SEM images (Fig. 3C and 3D). The presence of large cells can also show that a significant amount of CO_2 did not dissolve into the melt leading to pockets of extra gas accumulated leading to this irregular structure.

Comparing the results obtained at 110 and 130°C, it can be concluded that, in general, the system reacted to the changes in extrusion parameters in the same way at both temperatures. The effect of temperature on foaming was prominent: at the lower temperature, 110°C, the lower diffusivity could limit gas loss, and the remaining amount could contribute more to the volume expansion. The higher viscosity could prevent cells to coalesce, helped to freeze the cell walls and hence hindered cell collapse. Finally, these led to larger porosity, thinner cell walls and better foam homogeneity.

Grindability

Post-processing of extruded solid dosage forms mostly involves a cutting and a grinding step. It is, therefore, an essential requirement that the extrudate should be rigid and fragile. Unfortunately, glass-transition temperature of polymer particles tends to decrease when particle diameter is decreased, especially when into the submicronic range, as investigated by *Wang et al*. for PVA fibers[49] (the usual diameter of electrospun fibres falls into the range of 50–500 nm[50]) It was, therefore, necessary to examine whether the produced foams were rigid and hence eligible for further processing. *Cho and Rizvi* have previously shown that breaking stress of foams depends on the ratio of cell wall thickness to cell diameter.[51] In the present work, a non-foamed formulation (S 130/1/250/0, Table 3), a low-porosity extrudate with thicker cell walls and irregular cell structure (S 130/1/250/6), and a high-porosity foam with thinner cell walls and tighter cell diameter distribution (S 110/10/150/3) were selected for testing.

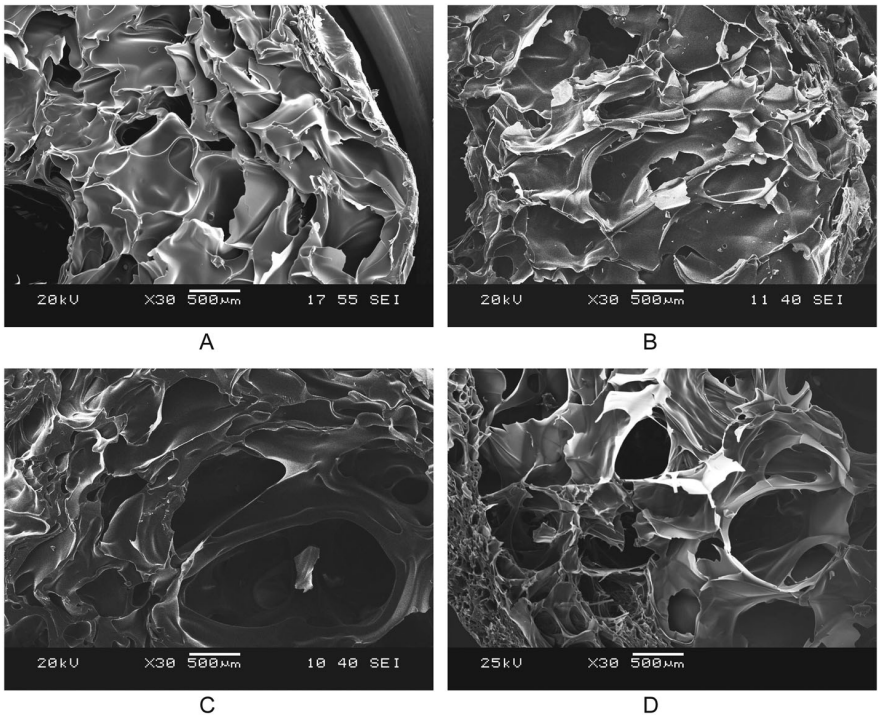

Figure 3. SEM image of (A) S 130/10/250/3, (B) S 130/10/250/6, (C) S 130/1/250/6 and (D) S 110/1/250/6.

Fragility of samples was characterized by three-point bending, measuring the flexural strength of the cylinder-shaped extrudate pieces. Table 4 shows that S 130/1/250/0 with 0% porosity required 14.63-MPa pressure to fracture at 1.51% strain, while S 130/1/250/6 with 64% porosity could be broken with 1.99 MPa at 2.26% strain. S 110/10/150/3 had the highest (92%) porosity and many submicronic cell walls, which made the sample reasonably more flexible, but it could still be fractured with 0.40 MPa at a strain of 7.87%. This shows that melt extrusion assisted by supercritical CO_2 can produce well-grindable submicronic or few-micronic (Fig. 4) structures with high specific surface area continuously, while fibre-forming technologies (e.g. electrostatic spinning), which are usually used for similar or the same formulation purposes, can have grindability issues at ambient temperature.[52]

Residual drug crystallinity in the formulations

Differential scanning calorimetry (DSC) is one of the conventional techniques that can be used to quantify or estimate crystallinity in extruded samples. In the case of spironolactone, the specific melting heat of the crystalline drug at 211°C was supposed to decrease with a decreasing degree of residual crystallinity. On the contrary, not even a physical mixture of 10% spironolactone and 90% Eudragit E released significant melting heat at that temperature. Most probably, Eudragit E, which reached glass-transition quite early around 50°C, dissolved the drug compound before the melting point could have been reached.

Because of the above mentioned uncertainty of DSC tests, crystallinity of extrudates was characterized using X-ray powder diffraction (XRPD, Fig. 5), which is another traditionally used technique for this purpose,[6,53] and Raman spectrometry (Fig. 7). In the case of XRPD, Eudragit E causes no diffraction while the crystalline API does. Should a sample be fully amorphous, only a very broad peak (halo) would be observed. As Fig. 5 shows, very small peaks could be discovered in all cases but one (S 130/1/250/6), which were quite difficult to distinguish from the noise due to their low intensity. This indicates that residual crystals are present to a small extent in the melt-extruded formulations. Taking into account the similarity of XRPD curves and the fact that extrusion temperature and melt throughput were varied widely in the region in which the spironolactone–Eudragit E system was processable, the findings indicate that full amorphization could nearly be obtained without further optimization, even at the high drug loading used. Optimal operating conditions can be hence chosen by considering other factors, e.g. achievable purity.

Table 4. Flexural strengths of selected extrudates

Sample	Porosity (%)	Mean flexural strength (MPa)	Mean flexural strain (%)
S 130/1/250/0	0	14.63 ± 1.88	1.51 ± 0.10
S 130/1/250/6	64	1.99 ± 0.52	2.26 ± 0.76
S 110/10/150/3	92	0.40 ± 0.13	7.87 ± 3.00

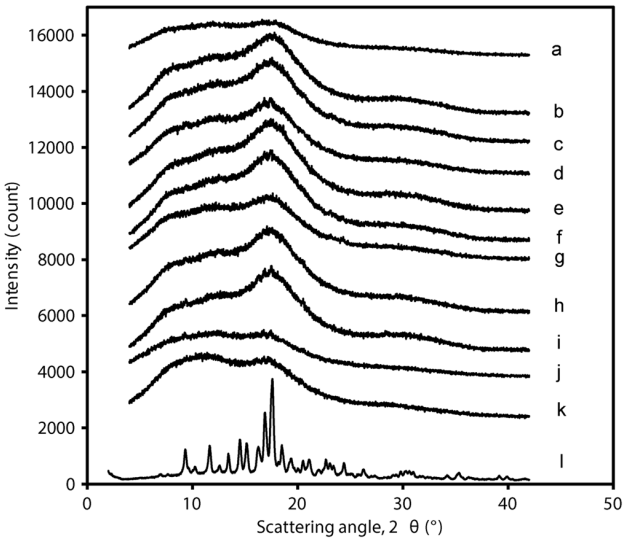

Figure 5. XRPD curves characterizing the crystallinity of extruded foams (a) Eudragit E, (b) S 130/1/250/6, (c) S 130/10/250/6, (d) S 130/10/250/3, (e) S 130/10/200/3, (f) S 130/10/150/3, (g) S 110/1/250/6, (h) S 110/6/250/6, (i) S 110/6/250/3, (j) S 110/6/200/3, (k) S 110/10/150/3 and (l) microcrystalline spironolactone.

Raman spectroscopy, which is another eligible technique to distinguish amorphous spironolactone from its crystalline form,[54] was used to observe the influence of extrusion conditions on amorphization and to estimate the crystalline/amorphous spironolactone ratio (C/A). As an in-line applicable tool, its use would be preferred to monitor continuous processing, according to PAT guidelines.[7] The scattering spectrum of the API changes when crystal lattice is destroyed. Crystals contain molecules in an arranged and repetitive structure; neighborhoods of Raman-active bonds are thus the same in each molecule. As the amorphous bulk has no ordered structure and neighborhoods are diverse, vibration energies are perturbed.[55] Therefore, the peak of spironolactone at 1690 cm^{-1}, which is assigned to the C=O bond of the thioacetyl group, broadens or merges with the peak at 1668 cm^{-1} when amorphization has taken place (Fig. 6).

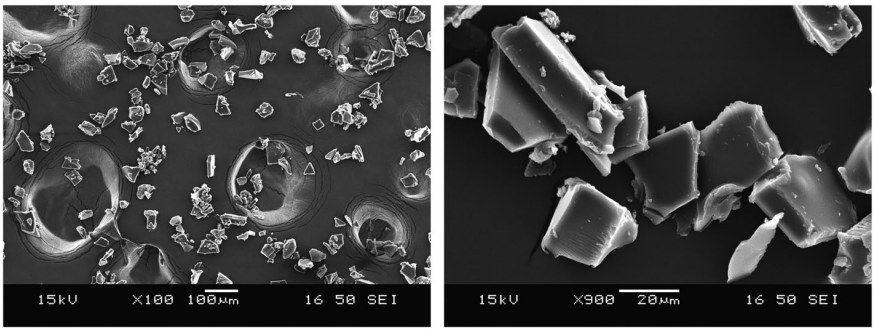

Figure 4. SEM images of ground S 110/6/250/6 extrudate ($d_p < 0.06$ mm). The larger circular spots belong to the adhesive tape.

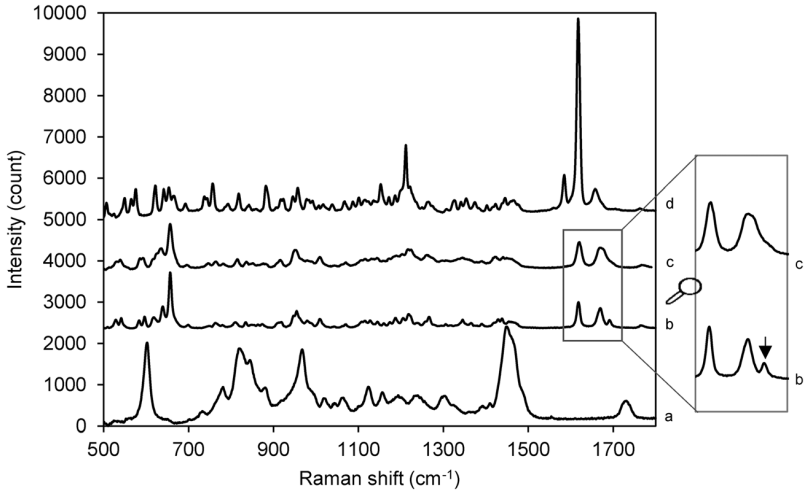

Figure 6. Raman spectrum of (a) Eudragit E, (b) crystalline spironolactone, (c) amorphous spironolactone prepared by electrospraying and (d) canrenone.

Confocal Raman mapping has the ability to characterize larger areas of investigated samples, which is utilized in chemical imaging[10] as well as to avoid subsampling. Extrudates prepared at different temperatures and throughputs were examined by performing three parallel Raman mappings for each extrusion parameter setting. One hundred mapping points were defined in a long (150 μm) distance from each other. The mean spectrum of each Raman map delivered a crystalline/amorphous spironolactone CLS score ratio. Figure 7 shows the calculated C/A values sorted by extrusion conditions.

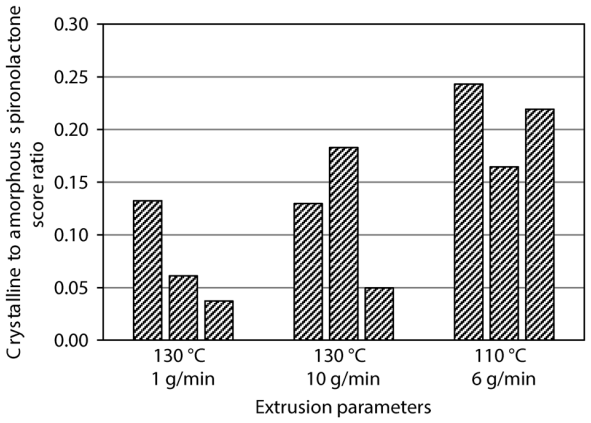

Figure 7. CLS score ratios of crystalline and amorphous spironolactone (C/A) in the case of various foams, measured by Raman mapping. Three parallel samples were tested for each parameter setting.

C/A was low, around 0.077 in the case of 10%-API formulations prepared at a temperature of 130°C and a thoughput of 1 g/min. When melt throughput was increased to 10 g/min, the shorter residence time resulted in slightly lower amorphicity, and hence slightly higher C/A. Results varied around 0.121 in this case. By decreasing temperature to 110°C and setting residence time to its achievable minimum (which was desirable considering drug degradation), the average C/A became 0.209. It can be concluded that the employed matrix polymer could dissolve a high amount of spironolactone, leaving behind less than 20% of the API content as residual crystals at 10% drug loading.

This finding confirms the result obtained by solubility parameter calculations, namely that strong secondary interactions can form between spironolactone and Eudragit E, making them highly miscible. Besides the thermodynamics of the process, the conclusions drawn based on Fig. 7 point out that the kinetics of drug dissolution in the melt, which is connected to residence time, is a non-negligible factor of amorphization either, because of the high viscosity of the melt and hence the slower diffusion of dissolved molecules from the crystal surface layer. In Fig. 7, it can also be observed that when more residual crystals were

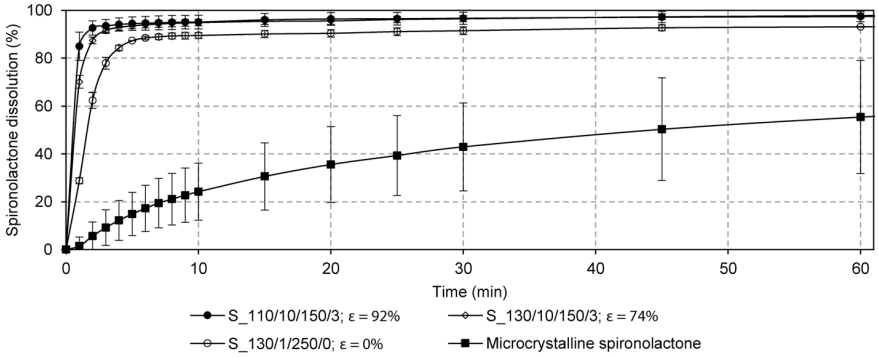

Figure 8. Dissolution of spironolactone from extruded formulations in comparison with the curve belonging to pure microcrystalline spironolactone. Intervals belonging to ± SD of three tests are shown. Dissolved amounts were compared to the total amount of spironolactone that was present in the tested samples (dissolved amounts after 8 h).

present in the system, formulations were not completely homogeneous. The fact that no considerable inhomogeneity could be observed in the distribution of degraded drug (purity results section) indirectly confirms that canrenone content originates primarily from molecularly dispersed spironolactone, while crystalline API remains stable in its crystal lattice.

Dissolution tests

The degree of dissolution enhancement achieved by forming solid dispersions was characterized with *in vitro* dissolution tests by carrying out three parallel measurements for each sample. In comparison with the extremely slow dissolution rate of microcrystalline spironolactone (Fig. 8), the dissolution of ground S 130/1/250/0 was fast. Partial amorphization of spironolactone and the solubilizing effect of Eudragit E enabled the immediate release of approx. 90% of the API content in 10 min. The larger crystalline drug particles from S 130/1/250/0 dissolved notably slower afterward.

Rapid dissolution was observed for the foamed samples (S 130/10/150/3 and S 110/10/150/3). It can be seen that dissolution was significantly faster in the case of S 110/10/150/3 having higher (92%) porosity than that of S 130/10/150/3 with 74% porosity despite the fact that residual drug crystallinity was higher in S 110/10/150/3.

CONCLUSION

The growing interest in melt extrusion in pharmaceutical development and drug manufacture is indicated by the high number of scientific papers published about the achievable benefits of this continuous technology. At the same time, the possible disadvantages as well as the ways to overcome these are less frequently discussed. Decomposition of heat-sensitive APIs and the difficulty of amorphization in the case of higher drug loadings are considered to be the major issues of conventional melt extrusion.

This study proved through the example of spironolactone–Eudragit E foamed solid dispersions that melt extrusion assisted by supercritical (sc) CO_2 injected into the melt can have significant benefits regarding product properties. The degree of API decomposition could be lowered because $scCO_2$ enabled processing at lower temperature ranges and high melt throughput. As a physical blowing agent, $scCO_2$ increased the specific surface area of the extrudates remarkably. The effect of temperature was found to be of major importance, and by optimization, 87–92% porosity and submicronic cell walls could be obtained. The increased specific surface area and the formation of highly amorphous solid dispersions made possible to achieve $>$90% drug release in 2 min in acidic medium.

The results presented here can contribute to a deeper understanding of the effect of extrusion parameters on decomposition processes occurring in the course of melt extrusion. The suppression of degradation reaction leading to higher purity, achievable by supercritical extrusion, can extend the circle of melt extrudable compounds.

Acknowledgements

This work was carried out in the Hungarian–French Scientific and Technological Cooperation project "New continuous polymer processing with supercritical fluids for pharmaceutical applications" (Project IDs: TÉT 11 2-2012-0014 and PHC Balaton 27862TG) funded by the National Development Agency of Hungary and Campus France. It is also connected to the scientific program of the "Development of quality-oriented and harmonized R + D + I strategy and functional model at BME" project. This work was financially supported by the New Széchenyi Development Plan (TÁMOP-4.2.1/B-09/1/KMR-2010-0002) and by the OTKA research fund (grant number PD108975) of the Hungarian Academy of Sciences. The authors mean to express their gratitude to Dr János Madarász and Márta Fejős for their assistance in XRPD measurements and mechanical testing, respectively. We are thankful to James Ferguson (The University of Edinburgh) for his assistance in language revision and to Tamás Amriskó, Laurent Devriendt and Bruno Boyer for their technical help.

REFERENCES

[1] Z. K. Nagy, A. Balogh, B. Vajna, A. Farkas, G. Patyi, Á. Kramarics, G. Marosi, *J. Pharm. Sci.* **2012**, *101*, 322 332. DOI: 10.1002/jps.22731
[2] M. M. Crowley, F. Zhang, M. A. Repka, S. Thumma, S. B. Upadhye, S. K. Battu, J. W. McGinity, C. Martin, *Drug Dev. Ind. Pharm.* **2007**, *33*, 909 926. DOI: 10.1080/03639040701498759
[3] M. A. Repka, S. K. Battu, S. B. Upadhye, S. Thumma, M. M. Crowley, F. Zhang, C. Martin, J. W. McGinity, *Drug Dev. Ind. Pharm.* **2007**, *33*, 1043 1057. DOI: 10.1080/03639040701525627
[4] Z. K. Nagy, K. Nyúl, I. Wagner, K. Molnár, G. Marosi, *Express Polym. Lett.* **2010**, *4*, 763 772. DOI: 10.3144/expresspolymlett.2010.92
[5] P. Kocbek, S. Baumgartner, J. Kristl, *Int. J. Pharm.* **2006**, *312*, 179 86. DOI: 10.1016/j.ijpharm.2006.01.008
[6] C. Mártha, L. Kürti, G. Farkas, O. Jójárt Laczkovich, B. Szalontai, E. Glässer, M. A. Deli, P. Szabo Revesz, *Eur. Polym. J.* **2013**, *49*, 2426 2432. DOI: 10.1016/j.eurpolymj.2013.03.006
[7] U.S. Department of Health and Human Services, Food and Drug Ad ministration, **2004**, http://www.fda.gov/downloads/Drugs/Guid ances/ucm070305.pdf Date accessed: 11 02 2014.
[8] J. Breitenbach, *Eur. J. Pharm. Biopharm.* **2002**, *54*, 107 117. DOI: 10.1016/S0939 6411(02)00061 9
[9] J. Breitenbach, *Am. J. Drug Deliv.* **2006**, *4*, 61 64. DOI: 10.2165/00137696 200604020 00001
[10] B. Vajna, H. Pataki, Z. Nagy, I. Farkas, G. Marosi, *Int. J. Pharm.* **2011**, *419*, 107 113. DOI: 10.1016/j.ijpharm.2011.07.023
[11] J. C. DiNunzio, C. Brough, J. R. Hughey, D. A. Miller, R. O. Williams III, J. W. McGinity, *Eur. J. Pharm. Biopharm.* **2010**, *74*, 340 351. DOI: 10.1016/j.ejpb.2009.09.007
[12] J. E. Patterson, M. B. James, A. H. Forster, R. W. Lancaster, J. M. Butler, T. Rades, *Int. J. Pharm.* **2007**, *336*, 22 34. DOI: 10.1016/j.ijpharm.2006.11.030
[13] J. R. Hughey, J. M. Keen, C. Brough, S. Saeger, J. W. McGinity, *Int. J. Pharm.* **2011**, *419*, 222 230. DOI: 10.1016/j.ijpharm.2011.08.007
[14] E. Petritz, T. Tritthart, R. Wintersteiger, *J. Biochem. Biophys. Methods* **2006**, *69*, 101 112. DOI: 10.1016/j.jbbm.2006.03.007
[15] A. Krupa, D. Majda, R. Jachowicz, W. Mozgawa, *Thermochim. Acta* **2010**, *509*, 12 17. DOI: 10.1016/j.tca.2010.05.009
[16] F. Kayaci, Y. Ertas, T. Uyar, *J. Agric. Food Chem.* **2013**, *61*, 8156 8165. DOI: 10.1021/jf402923c
[17] Z. K. Nagy, M. Sauceau, K. Nyúl, E. Rodier, B. Vajna, G. Marosi, J. Fages, *Polym. Adv. Technol.* **2012**, *23*, 909 918. DOI: 10.1002/pat.1991
[18] S. Li, M. Xiao, Y. Guan, D. Wei, H. Xiao, A. Zheng, *Eur. Polym. J.* **2012**, *48*, 362 371. DOI: 10.1016/j.eurpolymj.2011.11.015
[19] G. Verreck, A. Decorte, K. Heymans, J. Adriaensen, D. H. Liu, D. L. Tomasko, A. Arien, J. Peeters, G. Van den Mooter, M. E. Brewster, *Int. J. Pharm.* **2006**, *327*, 45 50. DOI: 10.1016/j.ijpharm.2006.07.024
[20] A. Salerno, U. Clerici, C. Domingo, *Eur. Polym. J.* **2014**, *51*, 1 11. DOI: 10.1016/j.eurpolymj.2013.11.015
[21] G. Bánsághi, E. Székely, D. M. Sevillano, Z. Juvancz, B. Simándi, *J. Supercrit. Fluids* **2012**, *69*, 113 116. DOI: 10.1016/j.supflu.2012.05.016
[22] C. Ortuño, T. Duong, M. Balaban, J. Benedito, *J. Supercrit. Fluids* **2013**, *82*, 56 62. DOI: 10.1016/j.supflu.2013.06.005
[23] S. S. H. Rizvi, S. J. Mulvaney, A. S. Sokhey, *Trends Food Sci. Technol.* **1995**, *6*, 232 240. DOI: 10.1016/S0924 2244(00)89084 6
[24] M. Sauceau, J. Fages, A. Common, C. Nikitine, E. Rodier, *Prog. Polym. Sci.* **2011**, *36*, 749 766. DOI: 10.1016/j.progpolymsci.2010.12.004
[25] G. Verreck, A. Decorte, K. Heymans, J. Adriaensen, D. Cleeren, A. Jacobs, D. H. Liu, D. L. Tomasko, A. Arien, J. Peeters, P. Rombaut, G. Van den Mooter, M. E. Brewster, *Eur. J. Pharm. Sci.* **2005**, *26*, 349 58. DOI: 10.1016/j.ejps.2005.07.006

[26] G. Verreck, A. Decorte, K. Heymans, J. Adriaensen, D. Liu, D. L. Tomasko, A. Arien, J. Peeters, P. Rombaut, G. Van den Mooter, M. E. Brewster, *J. Supercrit. Fluids* **2007**, *40*, 153 162. DOI: 10.1016/j.supflu.2006.05.005
[27] G. Verreck, A. Decorte, H. Li, D. Tomasko, A. Arien, J. Peeters, P. Rombaut, G. Van den Mooter, M. E. Brewster, *J. Supercrit. Fluids* **2006**, *38*, 383 391. DOI: 10.1016/j.supflu.2005.11.022
[28] A. Dolenc, J. Kristl, S. Baumgartner, O. Planinsek, *Int. J. Pharm.* **2009**, *376*, 204 12. DOI: 10.1016/j.ijpharm.2009.04.038
[29] C. Nikitine, E. Rodier, M. Sauceau, J. J. Letourneau, J. Fages, *J. Appl. Polym. Sci.* **2010**, *115*, 981 990. DOI: 10.1002/app.31031
[30] M. D. Hargreaves, N. A. Macleod, M. R. Smith, D. Andrews, S. V. Hammond, P. Matousek, *J. Pharm. Biomed. Anal.* **2011**, *54*, 463 468. DOI: 10.1016/j.jpba.2010.09.015
[31] A. Aina, M. D. Hargreaves, P. Matousek, J. C. Burley, *Analyst* **2010**, *135*, 2328 2333. DOI: 10.1039/c0an00352b
[32] S. Šašić, S. Mehrens, *Anal. Chem.* **2011**, *84*, 1019 1025. DOI: 10.1021/ac202396u
[33] A. Heinz, M. Savolainen, T. Rades, C. J. Strachan, *Eur. J. Pharm. Sci.* **2007**, *32*, 182 192. DOI: 10.1016/j.ejps.2007.07.003
[34] Z. Német, G. C. Kis, G. Pokol, Á. Demeter, *J. Pharm. Biomed. Anal.* **2009**, *49*, 338 346. DOI: 10.1016/j.jpba.2008.11.033
[35] L. Nørgaard, M. T. Hahn, L. B. Knudsen, I. A. Farhat, S. B. Engelsen, *Int. Dairy J.* **2005**, *15*, 1261 1270. DOI: 10.1016/j.idairyj.2004.12.009
[36] E. Widjaja, P. Kanaujia, G. Lau, W. K. Ng, M. Garland, C. Saal, A. Hanefeld, M. Fischbach, M. Maio, R. B. H. Tan, *Eur. J. Pharm. Sci.* **2011**, *42*, 45 54. DOI: 10.1016/j.ejps.2010.10.004
[37] K. Nakamoto, T. Urasaki, S. Hondo, N. Murahashi, E. Yonemochi, K. Terada, *J. Pharm. Biomed. Anal.* **2013**, *75*, 105 111. DOI: 10.1016/j.jpba.2012.11.020
[38] H. Pataki, I. Markovits, B. Vajna, Z. K. Nagy, G. Marosi, *Cryst. Growth Des.* **2012**, *12*, 5621 5628. DOI: 10.1021/cg301135z
[39] H. Pataki, I. Csontos, Z. K. Nagy, B. Vajna, M. Molnar, L. Katona, G. Marosi, *Org. Process Res. Dev.* **2013**, *17*, 493 499. DOI: 10.1021/op300062t
[40] T. Seki, J. Mochida, M. Okamoto, O. Hosoya, K. Juni, K. Morimoto, *Chem. Pharm. Bull.* **2003**, *51*, 734 736. DOI: 10.1248/cpb.51.734
[41] J. L. Sutter, E. P. K. Lau, In: *Anal. Profiles Drug Subst.*, Vol. *4* (Ed.: F. Klaus), Academic Press, London, **1975**, pp. 431 451.
[42] M. Sauceau, C. Nikitine, E. Rodier, J. Fages, *J. Supercrit. Fluids* **2007**, *43*, 367 373. DOI: 10.1016/j.supflu.2007.05.014
[43] National Institute of Standards and Technology, http://webbook.nist.gov/chemistry/ Date accessed: 05/02/2014.
[44] R. Span, W. Wagner, *J. Phys. Chem. Ref. Data* **1996**, *25*, 1509 1596. DOI: 10.1063/1.555991
[45] M. Fukuda, N. A. Peppas, J. W. McGinity, *J. Control. Release* **2006**, *115*, 121 129. DOI: 10.1016/j.jconrel.2006.07.018
[46] D. W. Van Krevelen, *Properties of polymers: their correlation with chemical structure, their numerical estimation and prediction from additive group contributions*, Elsevier, Amsterdam, **1997**.
[47] H. E. Naguib, C. B. Park, U. Panzer, N. Reichelt, *Polym. Eng. Sci.* **2002**, *42*, 1481 1492. DOI: 10.1002/pen.11045
[48] C. B. Park, A. H. Behravesh, R. D. Venter, *Polym. Eng. Sci.* **1998**, *38*, 1812 1823. DOI: 10.1002/pen.10351
[49] W. Wang, A. H. Barber, *J. Polym. Sci. Part B Polym. Phys.* **2012**, *50*, 546 551. DOI: 10.1002/polb.23030
[50] M. Fejős, K. Molnár, J. Karger Kocsis, *Materials (Basel).* **2013**, *6*, 4489 4504. DOI: 10.3390/ma6104489
[51] K. Y. Cho, S. S. H. Rizvi, *Food Res. Int.* **2009**, *42*, 603 611. DOI: 10.1016/j.foodres.2008.12.015
[52] G. Verreck, I. Chun, J. Rosenblatt, J. Peeters, A. Van Dijck, J. Mensch, M. Noppe, M. E. Brewster, *J. Control. Release* **2003**, *92*, 349 360. DOI: 10.1016/S0168 3659(03)00342 0
[53] M. Poostforush, H. Azizi, *eXPRESS Polym. Lett.* **2014**, *8*, 293 299. DOI: 10.3144/expresspolymlett.2014.32
[54] T. Vigh, T. Horváthová, A. Balogh, P. L. Sóti, G. Drávavölgyi, Z. K. Nagy, G. Marosi, *Eur. J. Pharm. Sci.* **2013**, *49*, 595 602. DOI: 10.1016/j.ejps.2013.04.034
[55] O. Rajabi, F. Tayyari, R. Salari, S. F. Tayyari, *J. Mol. Struct.* **2008**, *878*, 78 83. DOI: 10.1016/j.molstruc.2007.07.043

SUPPORTING INFORMATION

Additional supporting information may be found in the online version of this article at the publisher web-site.